Available online at www.sciencedirect.com
ScienceDirect
Journal of Magnetic Resonance 186 (2007) 228–237
JMR Journal of Magnetic Resonance
www.elsevier.com/locate/jmr

Spin state selective Hadamard encoding during transfer periods using multiple selective CW-HCP

Kyryl Kobzar, Burkhard Luy *

Department Chemie, Organische Chemie II, Technische Universität München, Lichtenbergstrasse 4, D-85747 Garching, Germany

Received 13 February 2007; revised 1 March 2007
Available online 12 March 2007

Abstract

Hadamard spectroscopy today represents an alternative to conventional Fourier transform spectroscopy. The selective inversion of several narrow frequency bands is typically achieved by taylored inversion pulses in place of t_1-evolution periods. However, band-selective inversion can also be achieved during coherence transfer steps, thereby shortening the period during which the magnetization is in the transverse plane. Using CW heteronuclear cross polarization (CW-HCP) as an example for highly selective coherence transfer, the implementation of Hadamard encoding within a transfer step is presented. Transfer characteristics, the preparation of multiple frequency selective CW-HCP and the possibility of acquiring spin state selective spectra are discussed in detail. The theoretical results are verified on two examples involving a cyclic pentapeptide and ubiquitin.

Keywords: Hadamard spectroscopy; CW; HCP; Multiple selective transfer; Spin state selectivity; IPAP

1. Introduction

In nuclear magnetic resonance, Hadamard encoding was first implemented in imaging applications [1–4] and has recently become a viable alternative to Fourier transform in multidimensional NMR spectroscopy [5–11]. If the resonance frequencies of desired signals are known, a set of multiple selective inversion pulses can be created and applied in a way that spectra are unambiguously reconstructed using the Hadamard transformation [12,13]. As in conventional multidimensional NMR spectroscopy, single scans add up constructively without loss in sensitivity, but the number of incremented 1D-spectra is only determined by the number of selectively inverted frequency regions and not by the sweep width and desired resolution. This can lead to significant reductions in measurement time especially for samples with few cross peaks and might also be used to selectively correlate a subset of signals [14,13] or to suppress water [15].

Hadamard encoding is usually achieved with a multiple selective inversion pulse applied instead of a t_1-evolution period [13]. The selectivity of the inversion pulse dictates the pulse length and is of similar duration as a constant time period with identical resolution. For larger molecules, however, this can affect signal intensity and shorter overall experiment times are generally desirable. One possibility for reducing experiment duration is the use of highly selective transfer building blocks for direct Hadamard encoding without additional inversion pulses. Such selective transfer is achieved, e.g. by double selective continuous wave heteronuclear cross polarization (CW-HCP) [16–18], for which a number of interesting applications has been shown [19–23], including spin state selective spectroscopy [24–26].

In the following, general technical details for Hadamard encoding via multiple selective transfer building blocks will be examined on the example of CW-HCP. Offset effects, modifications of the building block for selective inversion during transfer, requirements for phase alignment and the

* Corresponding author. Fax: +49 89 289 13210.
E-mail address: Burkhard.Luy@ch.tum.de (B. Luy).

1090-7807/$ - see front matter © 2007 Elsevier Inc. All rights reserved.
doi:10.1016/j.jmr.2007.03.004

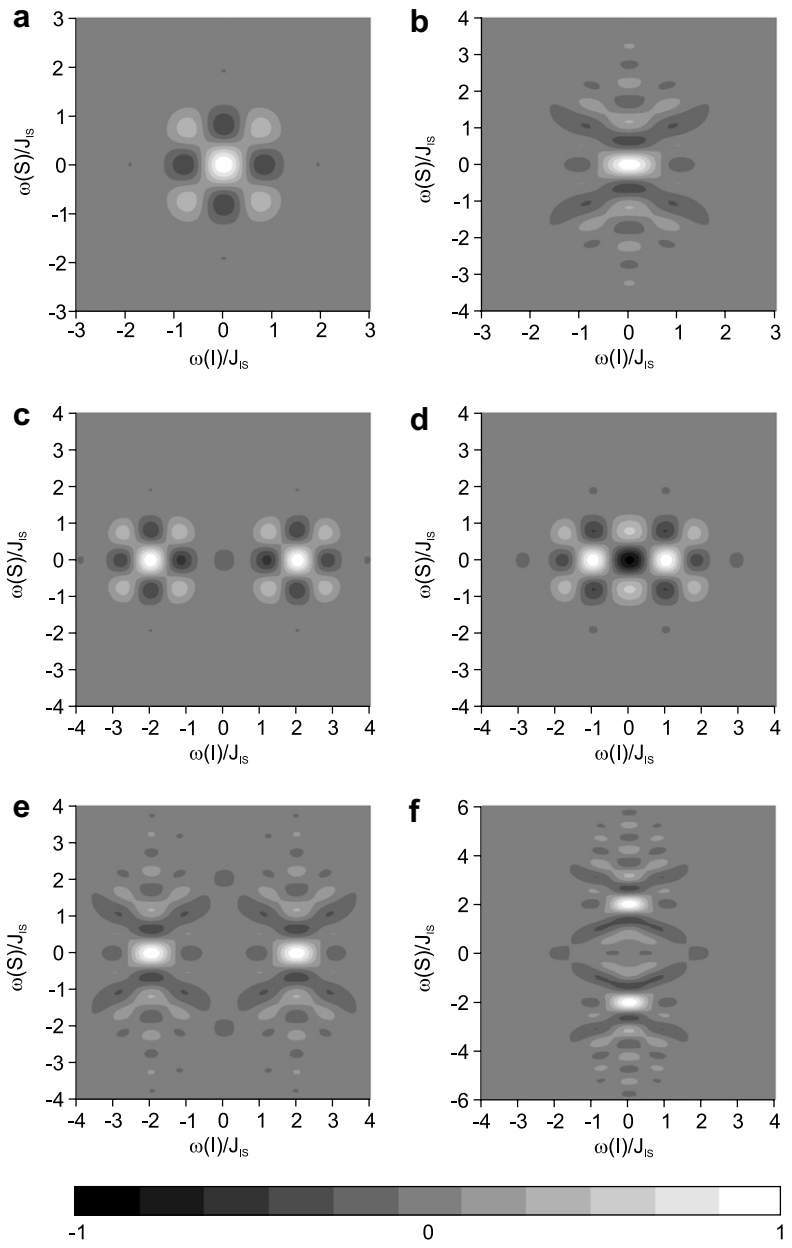

Fig. 1. Offset dependence of inphase to inphase and inphase to antiphase transfers using CW-HCP of duration $1/J$ applied in the following ways: (a) $S_x \xrightarrow{\mathrm{CW}_x(I,S)} I_x$; (b) $S_z \xrightarrow{\mathrm{CW}_x(I,S)} -2I_yS_x$; inphase to inphase transfer by irradiating at two offset frequencies ($\pm 2J$ (c) and $\pm$J (d)) on spin I with overall $\mathrm{rf}_{cw} = \sqrt{3}J/2$ while only one frequency is irradiated onresonant on spin S with $\mathrm{rf}_{cw} = \sqrt{3}J/4$; inphase to antiphase transfer by irradiating at two offset frequencies $\pm 2J$ with an amplitude $\mathrm{rf}_{cw} = \sqrt{3}J/2$ on the I (e) and S (f) spin, respectively, with the corresponding other spin irradiated onresonant with $\mathrm{rf}_{cw} = \sqrt{3}J/4$. The plots were simulated using self-written code based on the simulation program SIMONE [28,29].

application of spin state selectivity are discussed in detail. Results are verified experimentally on a ^{15}N, ^{13}C-labelled pentapeptide and uniformly ^{15}N, ^{13}C-labelled ubiquitin.

2. Theory

2.1. Transfer characteristics of CW-HCP

Continuous wave heteronuclear cross polarization (CW-HCP) has been shown in a nice series of publications to provide doubly selective transfer with a very narrow transfer bandwidth on both irradiated nuclei [17,18]. Best results are achieved for a radiofrequency amplitude of $\mathrm{rf}_{cw} = \sqrt{3}J/4$ with J being the active coupling between the two coupled spins. This low rf-amplitude results onresonant in a planar Hamiltonian [27]

$$\mathcal{H}_p^x = \pi J\{I_yS_y + I_zS_z\} \tag{1}$$

with full transfer after a transfer period of $\tau = 1/J$. In contrast to conventional high-power CW-HCP, the low

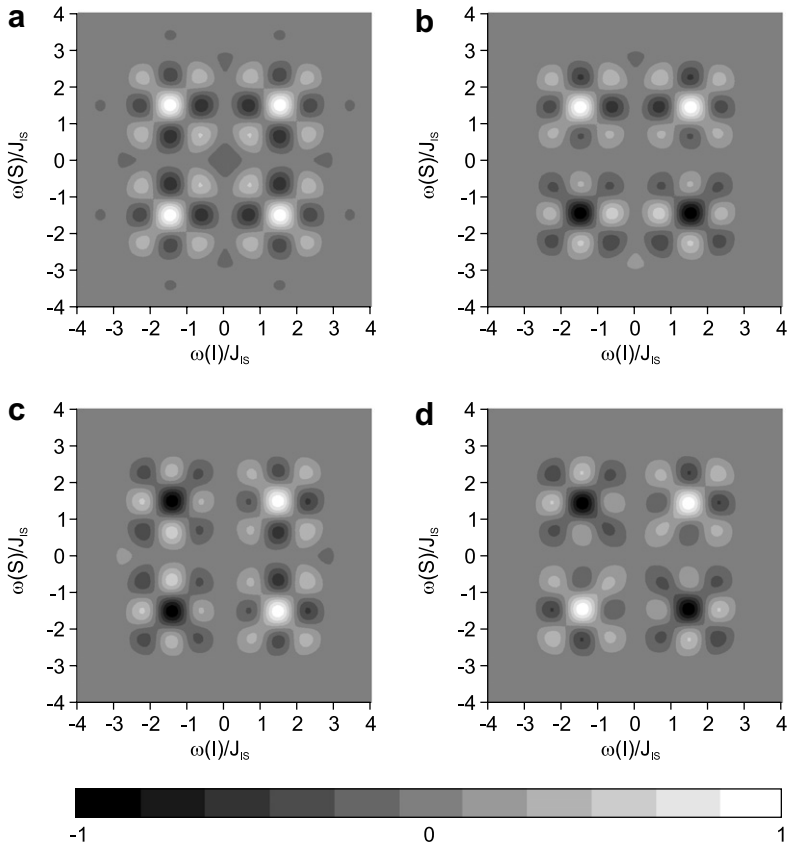

Fig. 2. Hadamard matrix encoding for dual selective inphase to inphase transfer using CW-HCP with selectively inverted CW-elements. All offset dependency plots were simulated with CW irradiated on I and S spins at frequencies of $\pm 1.5\,J$ with an overall amplitude of $\mathrm{rf_{cw}} = \sqrt{3}J/2$. While in (a) the phases of all CW-components have identical phases, the CW-component at frequency $-1.5\,J$ is inverted on the S spin (b), I spin (c), and both spins (d) to obtain the desired Hadamard-encoding during the multiple selective transfer period.

relative ratio of $\mathrm{rf_{cw}}$ and J yields a good compensation of B_1-field inhomogeneity [18]. Several transfers can be achieved with CW-HCP. The conventional application would be the transfer of inphase to inphase magnetization $I_x \rightarrow S_x$ via planar mixing as a result of CW_x-irradiation. However, if initial magnetization is oriented along z perpendicular to the irradiation axis, i.e. I_z, only the one component of the Hamiltonian orthogonal to both the irradiation and magnetization axes contributes to the transfer and weak coupling evolution takes place resulting in transfer from inphase into ZQ/DQ terms $I_z \rightarrow -2I_xS_y$ after $\tau = 1/J$. Since the ZQ/DQ term $2I_xS_y$ can easily be converted into antiphase magnetization by a simple 90° pulse, we will refer to this transfer as inphase to antiphase in the following. These two transfer pathways have already been used for reducing multiplets [27] and for bandwidth and spin state selective transfer [24–26] and will be discussed later in this article in terms of their applicability to multiple selective transfer.

The offset dependence of both transfer types is shown in Fig. 1a and b. The bandwidth of inphase to inphase coherence transfer is restricted to $\approx 0.55\,J$ with additional transition regions with undesired transfer up to approximately 2.4 J. The inphase to antiphase transfer has similar selectivity in the target dimension but a slightly more diffuse transition region in the initial dimension which, however, still provides sufficient selectivity for many applications.

CW-HCP transfer can be further manipulated by irradiating CW with a shifted phase on the second nucleus. The resulting onresonant transfers for an inverted, i.e. shifted by 180°, CW-irradiation on the S spin are $I_x \xrightarrow{CW_x(I)/CW_{-x}(S)} -S_x$ and $I_z \xrightarrow{CW_x(I)/CW_{-x}(S)} +2I_xS_y$ with the correspondingly inverted offset profiles. Since the rotating frames of the two heteronuclei are independently defined, the shift of the director of the CW-irradiation generally results in a phase shift of the evolving coherences.

2.2. Multiple selective CW-HCP and Hadamard encoding

Multiple selective CW-HCP can be achieved by the addition of several constant amplitude pulses with differing linear phase sweeps corresponding to the desired multiple frequencies. The creation of such a pulse shape is easily performed using standard procedures implemented for example in the Bruker pulse "shape tool" software as part of the XWINNMR program and is shown schematically

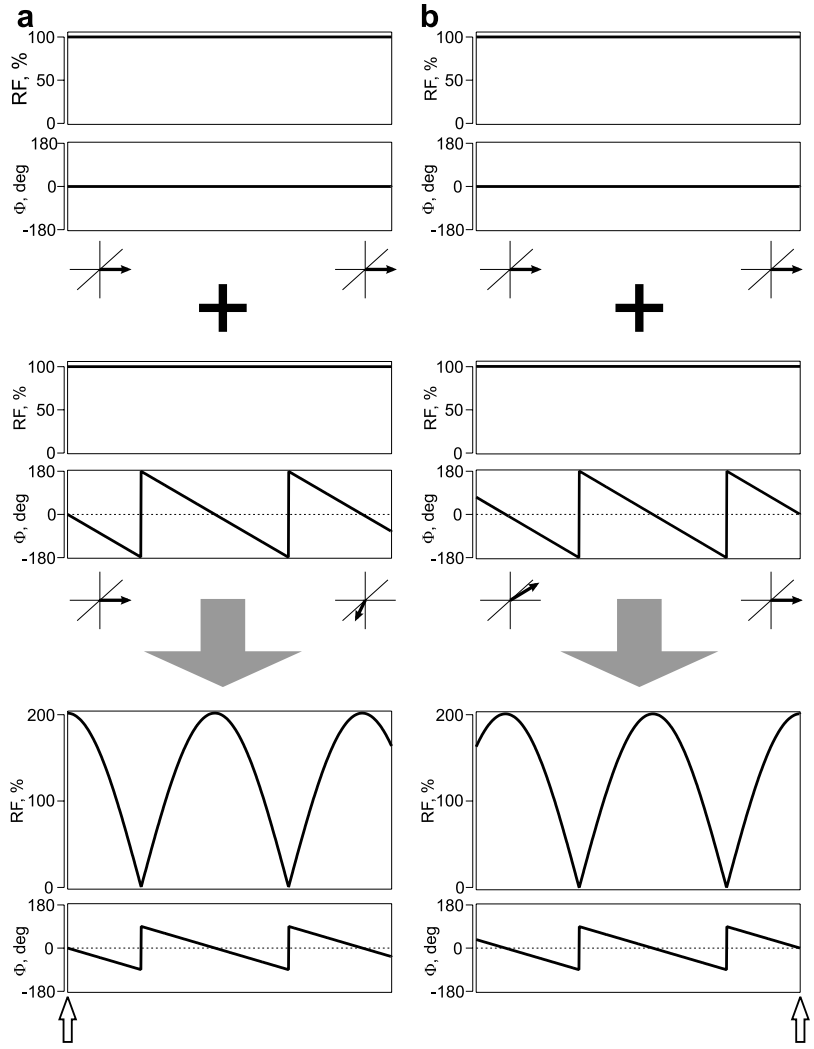

Fig. 3. Vector addition and phase alignment for multiple selective CW-HCP demonstrated by the addition of two constant amplitude CW pulses. Onresonant CW with constant amplitude and phase (top) is added vectorially with CW of constant amplitude at a specific offset (middle) with phases of the individual pulses aligned along x (0°) at the beginning (a) and at the end (as also indicated by the open arrows at the very bottom). The resulting pulse shapes are cosine-modulated pulses with a constant phase sweep of twice the original maximum rf-amplitude (bottom). Coordinate systems with a vector indicating the position of the CW-rotating frame have been introduced to visualize the relative phases at the beginning and at the end of the individual pulses.

for two frequencies in Fig. 3. Generally, for n separated irradiation frequencies on one nucleus the rf-amplitude also increases to n times rf_{cw}.

The multiple selectivity can be chosen independently for the two nuclei. Fig. 1c–e contains examples where two frequencies are chosen for spin I, while only one frequency is selected for the S spin for inphase to inphase and inphase to antiphase transfer, respectively. Inphase to antiphase transfer with one frequency on the I spin but two irradiated frequencies on the S spin is shown in Fig. 1f. In the case of two selected frequencies as shown in Fig. 2a, transfer can occur between all four frequency combinations. If a constant amplitude pulse at a single frequency is added with a 180° phase shift for the multiple selective CW pulse, the transfer at this specific frequency is also inverted (Fig. 2b–d).

The obtained offset dependencies for multiple CW-irradiation are the sum of the individual CW-HCP offset dependencies centered at the specified frequency combinations of I and S spins. Overlap of transfer regions between two neighboring CW-frequencies leads to incomplete or undesired transfer properties and should strictly be avoided. If the minimum distance of 1.8 J between two irradiation frequencies is maintained, clean multiple selective CW-HCP is achieved.

Hadamard spectra can be obtained with the S spin in the indirect dimension by encoding positive and negative transfers [1,31]. This can be achieved by addition and subtraction of the corresponding frequency components in the pulse shapes for the I and S spin as described above. The most simple non-trivial case of two selected frequencies for both the I and S nuclei is shown with its offset dependency plots in

Fig. 2. With the combination of all positive transfers (Fig. 2a), selective inversion of a single frequency on the I spin, S spin, and both spins (Fig. 2b–d), the spectra at all four frequency-combinations can be reconstructed [30,31]. The Hadamard encoding can be extended to $4n$ selected irradiation frequencies by adding and subtracting the phase-modulated CW-elements in the multiple selective CW-HCP according to the corresponding Hadamard matrices [13].

2.3. Phase alignment

When setting up experiments, special care has to be taken with respect to the correct phase alignment when creating the multiple selective CW-shaped pulses. Because CW of different frequencies is added for the CW-HCP, a defined phase is only provided at a single point of the resulting shapes, typically at the beginning or at the end of the shaped pulse (see Fig. 3 for a simple vector addition of two CW frequencies). Magnetization oriented along z obviously is not sensitive with respect to phase alignment. Transverse coherences, instead, only result in defined transfers for the specified frequencies if the corresponding pulse phases are identical. For the transfer $I_x \rightarrow S_x$, for example, the phases of the individual constant amplitude CW-pulses have to be aligned at the beginning of transfer step for the I spin, while they have to be aligned at the end of the pulse shape for the S spin. The inphase to antiphase transfer $I_z \rightarrow 2I_xS_y$ requires phase alignment at the end of the shaped pulse for both spins. Two pulse sequences for Hadamard encoded multiple selective CW-HCP based correlation experiments with inphase and antiphase detection, respectively, are presented in Fig. 4, with phase alignment of the multiple selective CW indicated by open arrows.

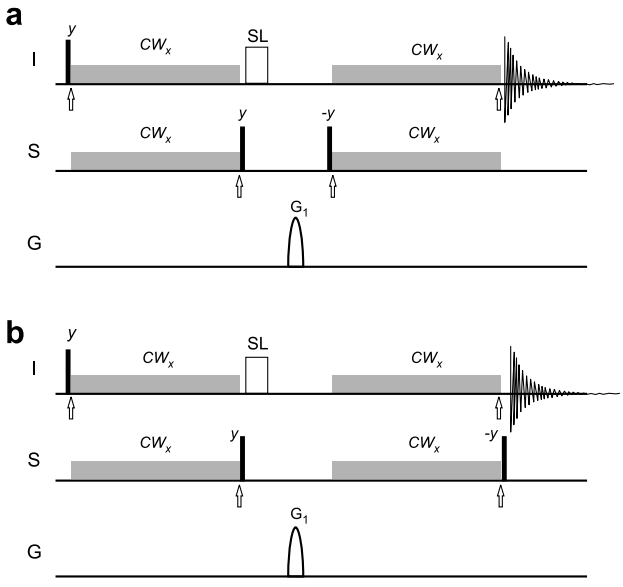

Fig. 4. Pulse sequences for Hadamard-encoded multiple selective CW-HCP correlations. (a) Sequence for the detection of inphase magnetization and (b) the corresponding sequence for antiphase detection. Open arrows indicate points of phase alignment of the multiple selective CW-HCP shaped pulses as demonstrated in Fig. 3. Black bars represent 90° pulses, gray bars annotated with CW_x mark mutliple selective CW-irradiation with phase aligned along x at the open arrows and the open box with SL stands for a spinlock period of typically 1–2 ms duration. The CW$_x$-irradiation used for experiments in all presented cases has a duration of $1/J$. The purging gradient G_1 is of medium strength and typically 1–5 ms duration. With the magnetization of interest stored on spin S along z, the combination of spinlock and purging gradient is known to provide excellent suppression of unwanted signals [37,26]. Hadamard encoding is achieved within the CW-HCP pulse shapes as described in the text.

2.4. Spin state selectivity

For spin state selectivity with respect to the α and β states of the heteronucleus, the resulting antiphase spectrum is added or subtracted from the inphase spectrum. As shown previously [26,32–36], the combination of spin state selective heteronuclear transfer with an homonuclear mixing step like TOCSY provides the possibility to measure size and sign of long-range heteronuclear couplings.

3. Experimental

The applicability of the method is demonstrated on 2 mM uniformly ^{15}N, ^{13}C-labelled cyclic pentapeptide cyclo(-D-Pro-Ala-Ala-Ala-Ala-) (PA_4) in DMSO-d_6 (Fig. 5), as well as on 0.5 mM uniformly ^{15}N, ^{13}C-labelled ubiquitin dissolved in 90% D_2O/10% H_2O (Fig. 6).

The alanines of the pentapeptide PA_4 result in four ^{15}N-split doublets for the amide protons in the ^{1}H-1D. The inner two amide signals, however, are too close at a spectrometer frequency of 600 MHz to be separated by multiple selective CW-HCP regarding the heteronuclear coupling of $^1J_{NH} \approx 90$ Hz. While their separation of approximately 70 Hz in ^{1}H and 65 Hz in ^{15}N results in significantly reduced transfer if all four amide groups are irradiated simultaneously in the multiple selective transfer steps, full transfer can be achieved for three amide groups, if only one of the central signals is irradiated (Fig. 5b).

For the experimental verification of the multiple selective CW-HCP Hadamard encoding, we initially chose the most simple example corresponding to a 2×2 Hadamard matrix. The two outer amide groups separated by 584 Hz in ^{1}H and 530 Hz in ^{15}N at a 600 MHz spectrometer have been irradiated according to the pulse sequences shown in Fig. 4 and the multiple selective CW-HCP building blocks of 11.1 ms duration constructed according to Fig. 3 and Figs. 2a and b. Hadamard-encoded inphase to inphase and inphase to antiphase transfer could be achieved with the transfer elements as described in the theory section. The subsequent addition/subtraction of the corresponding spectra leads to individual inphase/antiphase signals and even to spin state selective spectra (Fig. 5c).

A more elaborate example was recorded on ubiquitin, where four cross peaks were arbitrarily chosen for selective transfer with relative frequencies of 0, 315, 527, 770 Hz on ^{1}H and 0, 628, 895, 1075 Hz on ^{15}N (Fig. 6). In order to

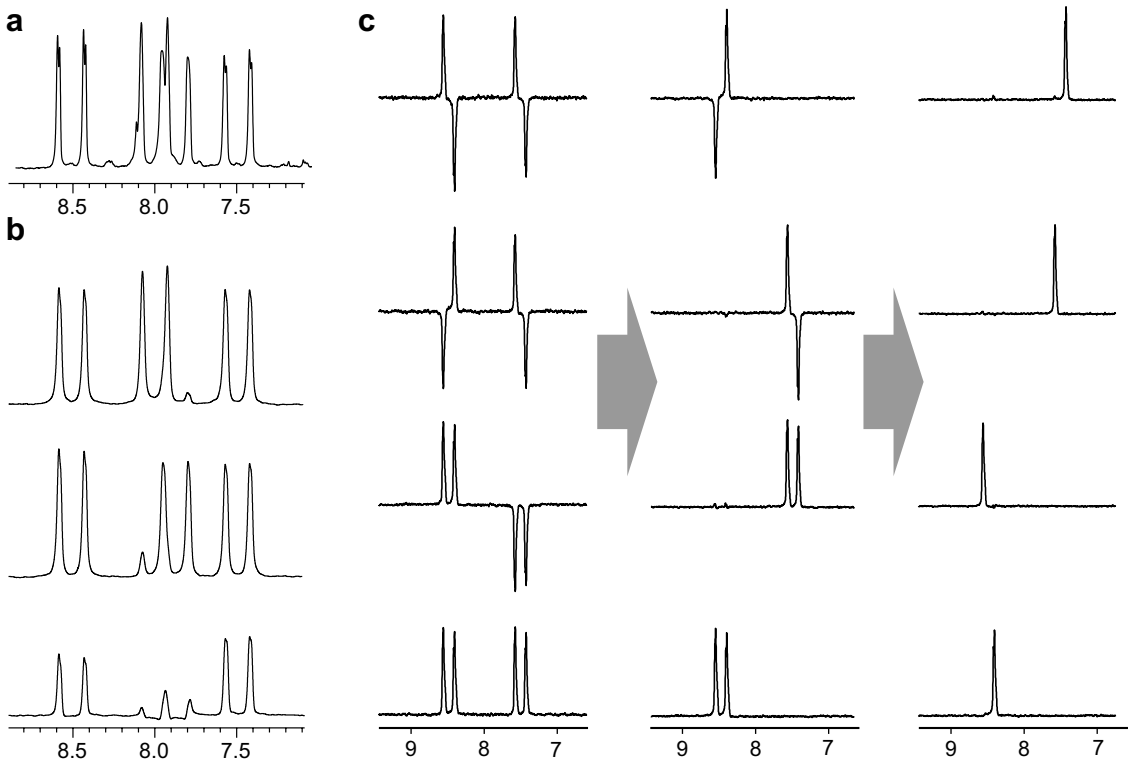

Fig. 5. Demonstration of achievable multiple selective CW-HCP transfer and a simple example for Hadamard-encoding including spin state selectivity using the ^{15}N, ^{13}C-labelled pentapeptide PA_4. (a) ^{1}H-1D of the amide region of PA_4. (b) While multiple selective ^{1}H,^{15}N CW-HCP cannot be achieved for all four alanine amide groups due to the insufficient separation of only $\approx 0.8\ ^1J_{NH}$ of the inner signals (bottom), it is well possible for three selected signals (top and middle). (c) Hadamard-encoding is demonstrated on the two outer amide signals for which inphase and antiphase detected experiments (Fig. 4) have been detected using twice-selective CW-HCP with all individual constant amplitude pulses added with the same phase (see Fig. 2a) and with one phase on spin S inverted before vector addition (see Fig. 2b). By applying the 2×2 Hadamard-matrix, which is equivalent to addition/subtraction of the two antiphase and inphase spectra, respectively, subspectra with individual antiphase/inphase signals are obtained. By combining these antiphase and inphase signals a second time in the IPAP manner, the four resulting subspectra represent the muliplet components of the individual spin states.

obtain maximum selectivity, Hadamard encoding was performed on both channels simultaneously [31], resulting in altogether 16 separate experiments for inphase spectra and another 16 experiments for antiphase spectra. These data have been combined by applying the Hadamard transformation using a 4×4 Hadamard matrix for each channel separately [31,14]. The encoded spectra are shown in Fig. 6b and c for the inphase and antiphase case, respectively. Again, these subspectra can be added/subtracted to achieve additional spin state selectivity (Fig. 6d). Clearly visible are also the selectivity limitations of the method for one of the obtained signals where the strong cross peak marked with an asterisk resonates at an offset combination in the transition region of CW-HCP (Fig. 1a). This leads to relatively efficient inphase transfer and the observed undesired signal. Because the offset dependence of inphase to antiphase transfer is different (Fig. 1b), the resulting antiphase spectra contain other undesired artefacts resulting from transfer of signals in the CW-HCP transition region.

All experiments were performed on a Bruker DMX 600 spectrometer. The multiple selective pulses for CW-HCP transfers were created using the Bruker "shape tool" software incorporated in XWINNMR version 3.5 by vector addition of square pulses with phase slopes corresponding to the desired irradiation offsets. As part of the shape tool also the phase alignment of the pulse shapes could be chosen as described in the theory section. The Hadamard encoding was achieved by adding additional 180° phase shifts to the corresponding individual frequency components. The pulse amplitudes were first set to theoretical values of $(\sqrt{3}/4)J_{NH}$ per irradiation frequency, and then corrected by systematically varying the amplitudes on both channels close to this value until reaching maximum signal intensity.

For PA_4, four scans per FID with 2048 points were recorded in all cases. The ^{1}H, ^{15}N-HSQC of ubiquitin was recorded with 2048×512 points and 4 scans per FID. The corresponding multiple selective CW-HCP Hadamard-encoded spectra were acquired with 8192 data points, 64 transients per individual experiment and CW-irradiation periods of 11.1 ms duration. Additional low-power presaturation was applied for water suppression in the case of ubiquitin. All spectra were zero-filled to twice

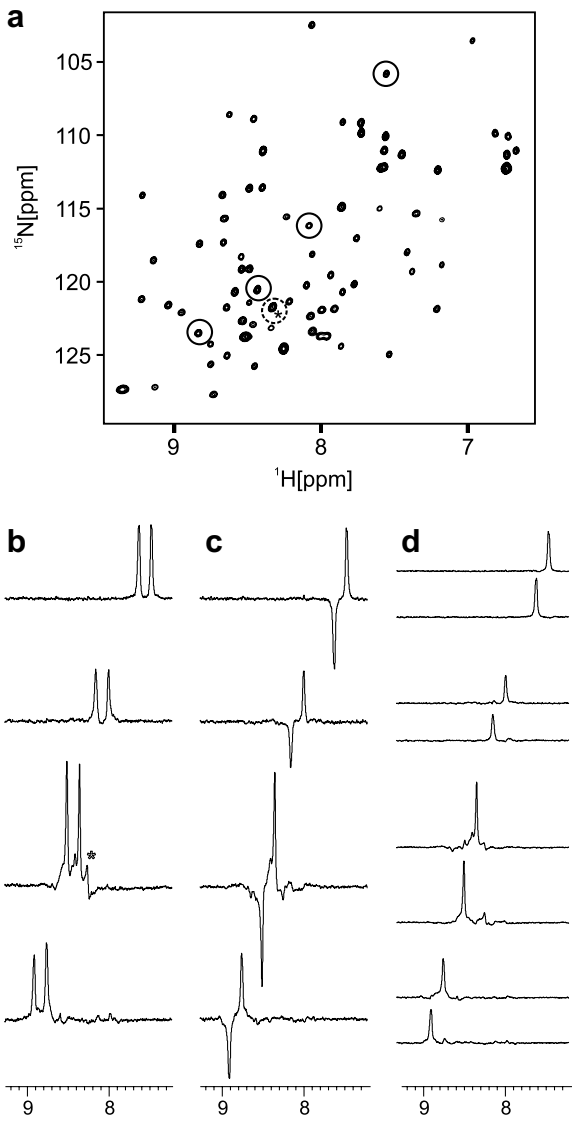

Fig. 6. Application of the multiple selective CW-HCP Hadamard encoding on ubiquitin by choosing four arbitrarily selected amide groups. (a) ^{1}H, ^{15}N-HSQC of ubiquitin with the four arbitrarily selected resonances indicated by circles. (b) The four resulting spectra out of 16 individually recorded inphase spectra using the pulse sequence of Fig. 4a after sequentially applying 4×4 Hadamard transformations on spins I (^{1}H) and S (^{15}N). (c) The corresponding spectra resulting from the 16 antiphase spectra recorded using the pulse sequence of Fig. 4b and corresponding Hadamard encoded CW-HCP. (d) By adding/subtracting inphase and antiphase spectra, individual multiplet components can be obtained. Limitations due to undesired transfer in the transition region of CW-HCP (see Fig. 1) are marked for the most pronounced case with an asterisk.

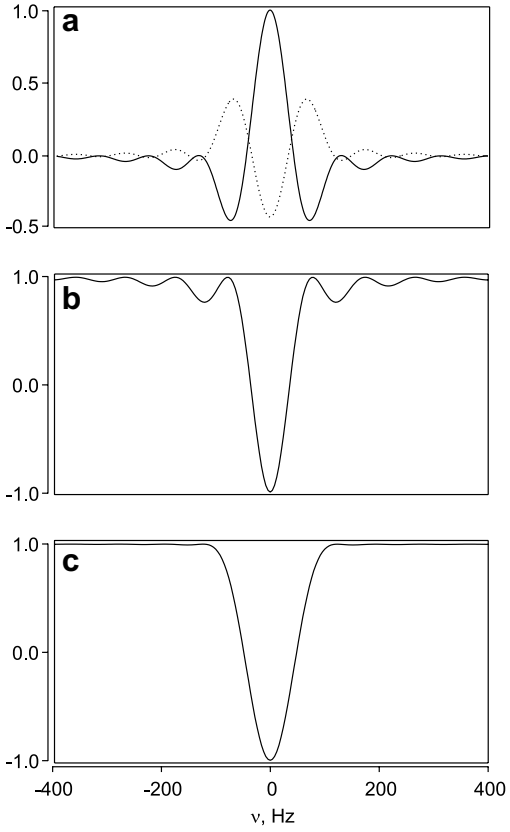

Fig. 7. Comparison of offset dependencies of CW-HCP (a), selective inversion using CW (b) and a selective inversion by Gaussian shaped pulse truncated at 15% (c). The duration of CW-HCP and the inversion pulses in all cases is 11.111 ms. For CW-HCP the transfer profile of the S spin is shown onresonant for the I spin (solid line) and for the I spin at an offset of $\approx 0.8\ J$ (dotted line, see Fig. 1a).

the original number of acquired points and apodized exponentially before Fourier transform.

4. Discussion

Highly selective CW-HCP has been shown to be a powerful tool for multiple selective Hadamard encoding. However, several limitations to the technique apply. The main disadvantage is probably the selectivity of transfer, which is limited by the heteronuclear coupling. Significantly narrower transfer bandwidths are only feasible using CW-HCP-based techniques with significantly longer transfer periods as for example described in [17,18,38,39]. These longer transfer periods will result in reduced transfer efficiencies due to relaxation.

Generally, it must be noticed that CW-HCP has quite large transition regions concerning its coherence transfer offset dependence (see Fig. 1). Other planar mixing schemes [40] optimized for selective coherence transfer, as e.g. the Gaussian pulse shape based PLUSH-TACSY [41] or the computer optimized kin-HEHAHA sequences [42], might well reduce resulting offset dependent artefacts. One could also think of optimizing selective heteronuclear or even homonuclear transfer building blocks by e.g. optimal control theory [43,44], which has shown its potential in many applications like the design of specific pulse shapes [45–48] or specifically optimized transfers in solid and liquid state applications [49–53].

A comparison of selectivity of CW-encoding vs. conventional Hadamard encoding using selective inversion pulses of identical duration is shown in Fig. 7. The selectivity of

CW-HCP is comparable to the selective inversion by a low-power CW pulse. Although the CW-transfer is not optimal with respect to the transition region, the actual transfer bandwidth is narrower as for example the bandwidth of a Gaussian inversion pulse with a truncation level of 15%. It can be assumed that the use of shaped pulses as e.g. applied in the PLUSH-TACSY [41] will lead to a reduced transition region also in the case of selective coherence transfer. Since physically the selectivity of a pulse sequence element is mainly determined by the time spent in the transverse plane, this result is not surprising. Potentially, the selectivity performance of a coherence transfer step might also be improved if the sequences irradiated on the two nuclei are treated separately in an optimization of band-selective transfer as has been previously demonstrated in [42].

In all multidimensional experiments coherence transfer steps are inevitable. The time for coherence transfer is not fully used in conventional Hadamard encoding procedures involving selective inversion pulses. In HSQC-type experiments, as shown here, a period of at least $1/J$ with the magnetization in the transverse plane can be gained by including the frequency selection into the transfer steps. This will generally result in higher sensitivity because of reduced relaxation losses. Most likely the two Hadamard encoding approaches can even be combined for obtaining spectra with higher selectivity and cleaner appearance.

Hadamard encoding with multiple selective CW-HCP requires several pulse shapes to be created for each 1D-experiment due to the various phase alignment conditions that must be fulfilled. The effort in this case is higher than in conventional Hadamard encoding schemes and is very time consuming if pulses are created individually. Nevertheless, pulse shape creation could easily be automated by a suitable computer program.

The original Hadamard encoding is restricted to frequency matrices that are multiples of $4n$. As has nicely been shown by Kupče and Freeman [54], the approach can be extended to an arbitrary number of frequencies, if not only sign inversion but encoding with $360°/n$ phase shifts is used. This extension can be directly transferred to multiple selective CW-HCP if the phases of the individual CW components are chosen accordingly.

In contrast to conventional Hadamard encoding using selective inversion pulses, multiple selective CW-HCP in principle offers the possibility to encode the frequencies of both participating nuclei without increase in experiment time for each scan. In the simple 2D-like correlation experiments discussed in Fig. 4, Hadamard encoding on both nuclei simultaneously is not necessary, since the proton dimension is directly detected anyway. In 3D-experiments the situation is different and the possibility of simultaneously encoding two frequency distributions in a single transfer element seems especially attractive in situations where fast relaxation processes limit the applicability of conventional frequency-discrimination techniques.

As mentioned above, the presented approach seems promising whenever relaxation prevents conventional Hadamard encoding using relatively long selective inversion pulses. The decrease in experiment time due to the inherent selectivity of the doubly selective CW-HCP will directly translate into gains in signal intensity. Possibly, the situation might be improved even further by the introduction of relaxation optimized transfer elements like the ROPE [55] and CROP [56] sequences, which both show an inherently bandwidth-selective transfer comparable to CW-HCP.

5. Conclusion

Using multiple selective continuous wave heteronuclear cross polarization, the idea of Hadamard encoding during a coherence transfer step was realized in theory and experiment. In this context, a number of technical details has been examined, like the bandselective sign-inversion of transfer and the offset dependent limitations for efficient transfer in multi-frequency CW. In addition, the role of phase alignment and the choice of corresponding transfer pathways for practical implementations have been discussed. The principles derived here for multiple selective CW-HCP are of general nature and should be applicable to many frequency selective transfer building block.

Acknowledgments

B.L. thanks the Fonds der Chemischen Industrie and the DFG for financial support (Emmy Noether fellowship LU 835/1).

References

[1] L. Bolinger, J.S. Leigh, Hadamard spectroscopic imaging (HSI) for multivolume localization, J. Magn. Reson. 80 (1988) 162–167.
[2] G. Goelman, V.H. Subramanian, J.S. Leigh, Transverse Hadamard spectroscopic imaging technique, J. Magn. Reson. 89 (1990) 437–454.
[3] G. Goelman, J.S. Leigh, B_1-insensitive hadamard spectroscopic imaging technique, J. Magn. Reson. 91 (1991) 93–101.
[4] R.A. de Graaf, Klaas Nicolay, Multislice imaging with adiabatic pulses using transverse Hadamard encoding, J. Magn. Reson. B 113 (1996) 97–101.
[5] L. Ma, P. Bigler, Simultaneous Measurement of one-bond and long-range carbon–carbon coupling constants in cembrene, Magn. Reson. Chem. 30 (1992) 1247–1254.
[6] C. Mueller, P. Bigler, Increased efficiency for the selective detection and measurement of carbon–carbon couplings, J. Magn. Reson. A 102 (1993) 42–48.
[7] V. Blechta, R. Freeman, Multi-site Hadamard NMR spectroscopy, Chem. Phys. Lett. 215 (1993) 341–346.
[8] V. Blechta, F. del Rio-Portilla, R. Freeman, Long-range carbon–proton couplings in strychnine, Magn. Reson. Chem. 32 (1994) 134–137.
[9] T. Nishida, G. Widmalm, P. Sandor, Hadamard long-range proton–carbon coupling constant measurement with band-selective proton decoupling, Magn. Reson. Chem. 33 (1995) 596–599.

[10] J. Schraml, H. van Halbeek, A. de Bruyn, R. Contreras, M. Maras, P. Herdewijn, Hadamard 1D ^{1}H TOCSY and its application to oligosaccharides, Magn. Reson. Chem. 35 (1997) 883–888.
[11] K. Krishnamurthy, Hadamard excitation sculpting, J. Magn. Reson. 153 (2001) 144–150.
[12] J. Hadamard, Résolution d'une question relative aux déterminants, Bull. Sci. Math. 17 (1893) 240–248.
[13] Ē. Kupče, T. Nishida, R. Freeman, Hadamard NMR spectroscopy, Prog. Nucl. Magn. Reson. Spectrosc. 42 (2003) 95–122.
[14] Ē. Kupče, R. Freeman, Fast multi-dimensional NMR of proteins, J. Biomol. NMR 25 (2003) 349–354.
[15] Ē. Kupče, R. Freeman, Frequency-domain Hadamard spectroscopy, J. Magn. Reson. 162 (2003) 158–165.
[16] S.R. Hartmann, E.L. Hahn, Nuclear double resonance in the rotating frame, Phys. Rev. 128 (1962) 2042–2053.
[17] E. Chiarparin, P. Pelupessy, G. Bodenhausen, Selective cross-polarization in solution state NMR, Mol. Phys. 95 (1998) 759–767.
[18] P. Pelupessy, E. Chiarparin, Hartmann-Hahn polarization transfer in liquids: an ideal tool for selective experiments, Conc. Magn. Reson. 12 (2000) 103–124.
[19] P. Pelupessy, E. Chiarparin, G. Bodenhausen, Excitation of selected proton signals in NMR of isotopically labeled macromolecules, J. Magn. Reson. 138 (1999) 178–181.
[20] O. Millet, E. Chiarparin, P. Pelupessy, M. Pons, G. Bodenhausen, Measurement of relaxation rates of N^{H} and N^{α} backbone protons with tailored initial conditions, J. Magn. Reson. 139 (1999) 434–438.
[21] E. Chiarparin, P. Pelupessy, B. Cutting, T.R. Eykyn, G. Bodenhausen, Normalized one-dimensional NOE measurement in isotopically labelled macromolecules using two-way cross-polarization, J. Biomol. NMR 13 (1999) 61–65.
[22] B. Cutting, G. Bodenhausen, Attenuation of cross-peak intensities in QUIET-BIRD-NOESY experiments, J. Magn. Reson. 140 (1999) 289–292.
[23] T.R. Eykyn, R. Ghose, G. Bodenhausen, Offset profiles of selective pulses in isotopically labelled macromolecules, J. Magn. Reson. 136 (1999) 211–213.
[24] T. Parella, J. Belloc, F. Sánchez-Ferrando, Measurement of the sign and the magnitude of heteronuclear coupling constants from spin-state-edited J-cross-polarization NMR experiments, Magn. Reson. Chem. 42 (2004) 852–862.
[25] T. Parella, Spin-state-selective excitation in gradient-selected heteronuclear cross-polarization NMR experiments, J. Magn. Reson. 167 (2004) 266–272.
[26] B. Luy, Spin state selectivity and heteronuclear Hartmann–Hahn transfer, J. Magn. Reson. 168 (2004) 210–216.
[27] T. Schulte-Herbrüggen, Z.L. Mádi, O.W. Sørensen, R.R. Ernst, Reduction of multiplet complexity in COSY-type NMR spectra. The bilinear and planar COSY experiments, Mol. Phys. 72 (1991) 847–871.
[28] S.W. Fesik, H.L. Eaton, E.T. Olejniczak, E.R.P. Zuiderweg, L.P. McIntosh, F.W. Dahlquist, 2D and 3D NMR-spectroscopy employing C-13–C-13 magnetization transfer by isotropic mixing-spin system identification in large proteins, J. Am. Chem. Soc. 112 (1990) 886–888.
[29] S.J. Glaser, G.P. Drobny, Assessment and Optimization of Pulse Sequences for Homonuclear Isotropic Mixing, in: W.S. Warren (Ed.), Advances in Magnetic Resonance, 14, Academic Press, New York, 1990, pp. 35–58.
[30] Ē. Kupče, R. Freeman, Two-dimensional Hadamard spectroscopy, J. Magn. Reson. 162 (2003) 300–310.
[31] Ē. Kupče, R. Freeman, Fast multi-dimensional Hadamard spectroscopy, J. Magn. Reson. 163 (2003) 56–63.
[32] A. Meissner, J.O. Duus, O.W. Sørensen, Spin-state-selective excitation. Application for E.COSY-type measurement of J(HH) coupling constants, J. Magn. Reson. 128 (1997) 92–97.
[33] M.D. Sørensen, A. Meissner, O.W. Sørensen, Spin-state-selective coherence transfer via intermediate states of two-spin coherence in IS spin systems: application to E.COSY-type measurement of J coupling constants, J. Biomol. NMR 10 (1997) 181–186.
[34] B. Luy, J.J. Barchi, J.P. Marino, S^{3}E-E.COSY methods for the measurement of ^{19}F associated scalar and dipolar coupling constants, J. Magn. Reson. 152 (2001) 179–184.
[35] K. Kobzar, B. Luy, Analyses, extensions and comparison of three experimental schemes for measuring ($^{n}J_{CH} + D_{CH}$)-couplings at natural abundance, J. Magn. Reson. 186 (2007) 131–141.
[36] T. Parella, A complete set of novel 2D correlation experiments based on heteronuclear J-cross polarization, J. Biomol. NMR 29 (2004) 37–55.
[37] B. Luy, G. Hauser, A. Kirschning, S.J. Glaser, Optimized NMR method for the configurational analysis of chemically equivalent vicinal protons, Angew. Chem. Int. Ed. 42 (2003) 1300–1302.
[38] F. Ferrage, T.R. Eykyn, G. Bodenhausen, Highly selective excitation in biomolecular NMR by frequency-switched single-transition cross-polarization, J. Am. Chem. Soc. 124 (2004) 2076–2077.
[39] F. Ferrage, T.R. Eykyn, G. Bodenhausen, Frequency-switched single-transition cross-polarization: a tool for selective experiments in biomolecular NMR, ChemPhysChem 5 (2004) 76–84.
[40] S.J. Glaser, J.J. Quant, Homonuclear and heteronuclear Hartmann–Hahn transfer in isotropic liquids, in: W.S. Warren (Ed.), Advances in Magnetic and Optical Resonance, 19, Academic Press, San Diego, 1996, pp. 59–252.
[41] T. Carlomagno, M. Maurer, M. Sattler, M.G. Schwendinger, S.J. Glaser, C. Griesinger, PLUSH TACSY: homonuclear planar TACSY with two-band selective shaped pulses applied to C_{α}, C' transfer and C_{β},$C_{aromatic}$ correlations, J. Biomol. NMR 8 (1996) 161–170.
[42] T. Carlomagno, B. Luy, S.J. Glaser, Kin HEHAHA Sequences, Heteronuclear Hartmann–Hahn transfer with different bandwidths for spins I and S, J. Magn. Reson. 126 (1997) 110–119.
[43] N. Khaneja, R. Brockett, S.J. Glaser, Time optimal control in spin systems, Phys. Rev. A 63 (2001) 032308.
[44] N. Khaneja, T. Reiss, C. Kehlet, T. Schulte-Herbrüggen, S.J. Glaser, Optimal control of coupled spin dynamics: design of NMR pulse sequences by gradient ascent algorithms, J. Magn. Reson. 172 (2005) 296–305.
[45] T.E. Skinner, T.O. Reiss, B. Luy, N. Khaneja, S.J. Glaser, Application of optimal control theory to the design of broadband excitation pulses for high resolution NMR, J. Magn. Reson. 163 (2003) 8–15.
[46] K. Kobzar, T.E. Skinner, N. Khaneja, S.J. Glaser, B. Luy, Exploring the limits of broadband excitation and inversion pulses, J. Magn. Reson. 170 (2004) 236–243.
[47] K. Kobzar, B. Luy, N. Khaneja, S.J. Glaser, Pattern pulses: design of arbitrary excitation profiles as a function of pulse amplitude and offset, J. Magn. Reson. 173 (2005) 229–235.
[48] T.E. Skinner, K. Kobzar, B. Luy, R. Bendall, W. Bermel, N. Khaneja, S.J. Glaser, Optimal control design of constant amplitude phase-modulated pulses: application to calibration-free broadband excitation, J. Magn. Reson. 179 (2006) 241–249.
[49] C. Kehlet, A.C. Sivertsen, M. Bjerring, T.O. Reiss, N. Khaneja, S.J. Glaser, N.C. Nielsen, Improving solid-state NMR dipolar recoupling by optimal control, J. Am. Chem. Soc. 126 (2004) 10202–10203.
[50] C. Kehlet, T. Vosegaard, N. Khaneja, S.J. Glaser, N.C. Nielsen, Low-Power homonuclear dipolar recoupling in solid-state NMR developed using optimal control theory, Chem. Phys. Lett. 414 (2005) 204–209.
[51] T. Vosegaard, C. Kehlet, N. Khaneja, S.J. Glaser, N.C. Nielsen, Improved excitation schemes for multiple-quantum magic-angle spinning for quadrupolar nuclei designed using optimal control theory, J. Am. Chem. Soc. 127 (2005) 13768–13769.
[52] N. Khaneja, J.-S. Li, C. Kehlet, B. Luy, S.J. Glaser, Broadband relaxation-optimized polarization transfer in magnetic resonance, Proc. Natl. Acad. Sci. USA 101 (2004) 14742–14747.

[53] D.P. Früh, T. Ito, Jr-Shin Li, G. Wagner, S.J. Glaser, N. Khaneja, Sensitivity enhancement in NMR of macromolecules by application of optimal control theory, J. Biomol. NMR 32 (2005) 23–30.
[54] Ē. Kupče, R. Freeman, Multisite correlation spectroscopy with soft pulses. A new phase-encoding scheme, J. Magn. Reson. A 105 (1993) 310–315.
[55] N. Khaneja, T. Reiss, B. Luy, S.J. Glaser, Optimal control of spin dynamics in the presence of relaxation, J. Magn. Reson. 162 (2003) 311–319.
[56] N. Khaneja, B. Luy, S.J. Glaser, Boundary of quantum evolution under decoherence, Proc. Natl. Acad. Sci. USA 100 (2003) 13162–13166.